Liquid Crystals
Publication details, including instructions for authors and subscription information:
http://www.informaworld.com/smpp/title~content=t713926090

Structure of the D phase. II

G. Etherington[ab]; A. J. Langley[a]; A. J. Leadbetter[a]; X. J. Wang[ac]
[a] Rutherford Appleton Laboratory, Chilton, Didcot, Oxfordshire, OX11 0QX, England [b] National Radiological Protection Board, Oxfordshire, England [c] Physics Department, Tsinghua University, Beijing, People's Republic of China

To cite this Article Etherington, G. , Langley, A. J. , Leadbetter, A. J. and Wang, X. J.(1988) 'Structure of the D phase. II', Liquid Crystals, 3: 2, 155 — 168
To link to this Article: DOI: 10.1080/02678298808086362
URL: http://dx.doi.org/10.1080/02678298808086362

LIQUID CRYSTALS, 1988, VOL. 3, NO. 2, 155–168

Structure of the D phase. II

by G. ETHERINGTON†, A. J. LANGLEY, A. J. LEADBETTER and X. J. WANG‡
Rutherford Appleton Laboratory, Chilton, Didcot, Oxfordshire OX11 0QX, England

(*Received 3 December 1986; accepted 26 July 1987*)

Results are presented of a Fourier analysis of quantitative X-ray diffraction data obtained from a D phase single crystal, the structure of which has previously been shown to possess primitive cubic symmetry. The Fourier analysis method determines the distribution of electron density in the crystallographic unit cell from the intensities and phases of the Bragg reflections. Diffraction data provide no information on the phase factors, and the Fourier method is therefore practical only when the structure is centrosymmetric, as is shown to be the case for the D phase, since the phase factors are then either 0 or π. It is shown that there are essentially only four physically reasonable solutions for the electron density distribution. The physical interpretation of these models is discussed in terms of molecular packing in the unit cell.

1. Introduction

In a previous paper [1], it was established for the first time, using X-ray diffraction data from a single crystal, that the so-called 'smectic D phase' has a three-dimensional primitive cubic crystalline structure. For 4-*n*-octadecyloxy-3′-cyanobiphenyl-4-carboxylic acid the unit cell dimension is 86 Å, which means that there are about 800 molecules per unit cell. The individual positions of the molecules are not definable, as is shown by the small number of Bragg reflections with observable intensities, and the phase is thus properly described as liquid crystalline. It is not, however, a smectic phase as its main structural feature is not a one-dimensional layer-like ordering.

The purpose of this paper is to present a quantitative analysis of the diffraction results, and to determine as much as possible about the structure. An important part of the analysis is the establishment of the centrosymmetric nature of the structure, which was achieved partly through measurements of the conversion efficiency of optical second harmonic generation.

2. Experimental

2.1. *X-ray measurements*

2.1.1. *Intensities*

Details of the sample, sample containment, the diffractometer and the X-ray area detector were given in the previous paper [1]. As discussed in that paper, by suitably orienting the sample it was possible to identify the stronger reflections from a single domain. The intensities of the Bragg reflections were measured by rocking the

† Present address: National Radiological Protection Board, Chilton, Didcot, Oxfordshire OX11 0RQ, England.
‡ Present address: Physics Department, Tsinghua University, Beijing, People's Republic of China.

cylindrical sample on the cylinder axis through each of the measurable reflections and, for each sample position, integrating over the region of the area detector where the background-subtracted intensity was significant. Intensity measurements were taken from the integrated intensity value at the peak of the rocking curve. Because of this, the Lorentz correction factor to the measured intensities was not necessary, while the polarization and absorption corrections were much smaller than experimental error. Table 1 gives the measured intensities.

Table 1. X-ray intensities. The intensities are normalized to $I_{200} = 1{\cdot}0000$. No {100} or {110} reflections were detected; their normalized intensities must be less than 10^{-4}. The errors for the {111}, {200}, {210} and {120} reflections are standard deviations, while the remaining values are estimated.

{*hkl*}	Number of reflections measured	Normalized Intensity	Error (%)
100	–	(0·0000)	–
110	–	(0·0000)	–
111	8	0·0395	14
200	4	1·0000	2
210	12	0·078	19
120	10	0·052	15
211	2	0·0024	50
220	2	0·0006	50
300	2	0·0052	20

2.1.2. *Correlation length*

The width of a Bragg reflection gives a measure of the correlation length L, a distance characterizing the extent of crystalline structural correlations and defined by

$$L = 1/(\Delta Q),$$

where $Q = 4\pi \sin\theta/\lambda$ and ΔQ is the half-width at half-maximum of the Bragg reflection. In fact, the diffraction peak widths are identical to the experimental resolution, so if it is assumed that the detection limit is 25% of the instrumental resolution, then the correlation length in the D phase must be greater than about 800 Å. The structure thus has three-dimensional correlations extending to at least 800 Å (or approximately ten unit cells). While this strongly suggests that the structure is a true crystal, a high-resolution diffraction experiment would be required to confirm this.

2.2. *Optical second harmonic generation measurements*

One of the conclusions of our earlier paper [1] was that the D phase is characterized by one of the five space groups P23, Pm3, P432, P$\bar{4}$3m and Pm3m. Diffraction techniques are not capable of distinguishing between these space groups, and an alternative technique is therefore needed. A narrowing of the choice of space groups can be made through the measurement of optical second harmonic generation, which is exhibited only by those primitive cubic structures with space group P23 or P$\bar{4}$3m. Second harmonic generation results from nonlinear terms in the electric susceptibility tensor, χ. In the general case the dominant contribution to second harmonic generation comes from second-order terms in χ, and in this approximation the nonlinear

polarization P^{NL} can be written as

$$P_i^{NL} = \chi''_{ijk} E_j E_k,$$

where χ'' is the second-order nonlinear susceptibility and is a third-rank tensor. From symmetry considerations, it can be shown that only for the non-centrosymmetric space groups P23 and P$\bar{4}$3m are any of the terms in χ''_{ijk} non-zero, while all the terms in χ'' are zero for the centrosymmetric space groups Pm3 and Pm3m as well as for the non-centrosymmetric space group P432. This is discussed by Nye [2], for the analogous case of the piezoelectric effect.

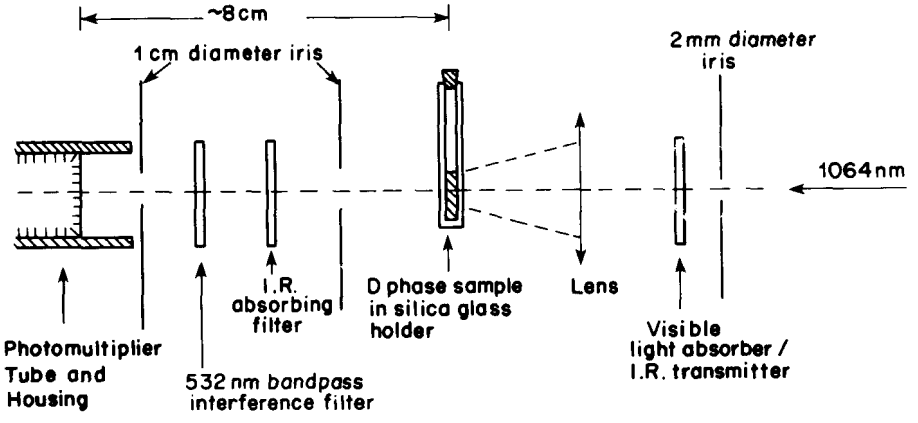

Figure 1. Experimental configuration for measurement of second harmonic generation.

To measure optical second harmonic generation, the experimental configuration shown in figure 1 was used. A filtered and partially focused I.R. beam from a Nd:YAG laser (λ = 1064 nm) was passed through a 1 mm thick D phase sample contained in a heated silica glass sample holder. The incident beam energy was 7 mJ/pulse, with a pulse width of approximately 10 ns. This is equivalent to an instantaneous peak power of approximately 700 kW, with $3{\cdot}7 \times 10^{16}$ photons per pulse. Any 532 nm second harmonic was filtered using a combination of an I.R. absorbing filter and a 532 nm bandpass interference filter, and detected using a high-sensitivity photomultiplier tube. With the simple detection electronics used, a maximum sensitivity of 3000 photons per pulse at 532 nm was obtained, corresponding to a conversion efficiency for second harmonic generation of about 10^{-13}.

A conversion efficiency of 4×10^{-12} was measured with the sample in the D phase, increasing to 10^{-11} when the sample was heated into the isotropic liquid phase. The conversion efficiency of a material that is not phase matched and has non-zero terms in the second-order nonlinear susceptibility tensor χ'' is expected to be in the range 10^{-7} to 10^{-8}. For an isotropic material such as a liquid, or for a centrosymmetric material, χ'' is zero. Any second harmonic generation must then arise principally from the quadrupole interaction corresponding to the fourth-rank tensor χ''' containing third-order nonlinear susceptibility terms. The conversion efficiency in this case is expected to be in the range 10^{-13} to 10^{-14}. It can be concluded that second harmonic generation in both the D phase and the isotropic phase arises from the quadrupole interaction. Thus P23 and P$\bar{4}$3m can be rejected as possible space groups. The slight increase in the conversion efficiency for the liquid can be accounted for by the higher optical transmission in this phase.

3. Results and discussion

3.1. *Space group*

In our earlier paper [1], P23 or Pm3 were considered to be the most likely of the five possible space groups for the D phase (P23, Pm3, P432, P$\bar{4}$3m or Pm3m), because of the small difference observed in the intensities of the {210} and the {120} reflections which implies a lack of fourfold symmetry. However, the {210} and {120} intensities differ from their average value by only 20%, which is close to the error limits of the measurements. If the constraint of the lack of fourfold symmetry is relaxed, the combined evidence from the diffraction and second harmonic generation experiments therefore indicates that the space group is Pm3, Pm3m or P432.

Of these, only P432 is non-centrosymmetric, and can be rejected as a possible space group for two reasons. Firstly, optical activity is exhibited by structures with P432 symmetry [2], and this was not detected in the D phase. Secondly, the smectic C phase, which is centrosymmetric, occurs at lower temperatures than the D phase in the compounds exhibiting the latter phase. The higher-temperature D phase would not be expected to have a lower degree of symmetry, so it must also be centrosymmetric. The space group must therefore be either Pm3 or Pm3m.

3.2. *Fourier synthesis of* $\varrho(\mathbf{r})$

Initially, several simple structural models, similar to those that have been discussed in the literature, were considered. For example, models where regions of high electron density can be represented by interconnecting rods [3], spherical micelles [4] or minimal surfaces [5, 6] were constructed. However, none gave a satisfactory fit to the experimental results.

A much more productive approach is to calculate, by means of Fourier inversion, the distribution of electron density in the unit cell, $\varrho(\mathbf{r})$. This distribution is related to the experimentally measured intensities by

$$\varrho(\mathbf{r}) - \varrho_0 = \sum_h \sum_k \sum_l \{|F(hkl)| \cos[2\pi(hx + ky + lz) - \phi_{hkl}]\}, \qquad (1)$$

where ϱ_0 is the average electron density, $|F(hkl)|$ is the modulus of the complex structure factor $F(hkl)$ and ϕ_{hkl} is the phase factor for the $\{hkl\}$ set of reflections. $|F(hkl)|$ is related to the measured intensity of the $\{hkl\}$ reflection by

$$|F(hkl)| = K(I_{hkl})^{1/2},$$

where K is a constant of proportionality.

In general, the phase factor ϕ_{hkl} for each reflection can take any value between 0 and 2π. As is well known, under normal experimental conditions no information on ϕ_{hkl} can be obtained, so it is not possible to compute $\varrho(\mathbf{r})$. However, if the space group is centrosymmetric, the phase factor ϕ_{hkl} must be either 0 or π. If, as is the case here, the number of reflections with measurable intensity is small, the problem is reduced to manageable proportions.

First, the electron density modelling for the space group Pm3m will be discussed; that is, under the assumption that $I_{210} = I_{120}$. Later the discussion will be generalized to include the space group Pm3; that is, $I_{210} \neq I_{120}$.

3.2.1. *Space group Pm3m*

For Pm3m, if the I_{210} value is taken to be the average of the measured intensities of the {210} and {120} reflections, there are six reflections with measurable intensities

Table 2. Relative contributions to $\varrho(\mathbf{r})$ from *hkl* reflections, Pm3m.

hkl	$\Delta\varrho$ (arbitrary units)
100	0
110	0
111	3·18
200	12·00
210	12·26
211	1·76
220	0·38
300	0·86

(see table 1). The relative contributions to $\varrho(\mathbf{r})$ from each can be seen from the quantity $\Delta\varrho$ ($=\varrho_{max} - \varrho_{min}$) shown in table 2, as calculated using equation (1). The three largest contributions are from the {111}, {200} and {210} reflections, and it is these that determine the qualitative characteristics of $\varrho(\mathbf{r})$.

Since the solution for $\varrho(\mathbf{r})$ depends only on the choice of 0 or π for each of the phase factors ϕ_{hkl}, the three strongest reflections yield only 2^3 ($\equiv 8$) possible models for $\varrho(\mathbf{r})$. This number is halved when an arbitrary choice of origin is allowed. Of the remaining four models, which may be labelled Models 1, 2, 3 and 4, two are simply the inverse of the remaining two in terms of electron density (i.e. $\varrho(\mathbf{r}) \rightarrow -\varrho(\mathbf{r})$). Consideration of the maximum and minimum values of $\varrho(\mathbf{r})$ enables the choice to be narrowed to two possible models, as follows.

The X-ray results give only relative values of electron density, but the ratio $r = (\varrho_0 - \varrho_{min})/(\varrho_{max} - \varrho_{min})$ calculated from the experimentally determined function $\varrho(\mathbf{r}) - \varrho_0$ may usefully be compared with values estimated for simple models. The experimental values for this ratio resulting from the four possible sets of phases for the different Bragg reflections are given in table 3.

The simplest—and also the most probable—structure to be associated with the maxima and minima of electron density are regions consisting respectively of all cores and all tails. The tendency of such aromatic and aliphatic regions to associate in this way is a well-defined feature of the packing of such molecules in both crystalline and

Table 3. Ratio $r = -\varrho_{min}/(\varrho_{max} - \varrho_{min})$ for the electron density models. The second set of phases for each model is equivalent to the first, with a shift of origin of $x = y = z = a_0/2$. Model 3 is the inverse of Model 1, while Model 4 is the inverse of Model 2 (e.g. $\varrho_3(\mathbf{r}) = -\varrho_1(\mathbf{r})$).

Model	ϕ_{200}	ϕ_{111}	ϕ_{210}	ϱ_{min}	ϱ_{max}	r
1	0	0	π	−6	10·53	0·363
	or 0	π	0			
2	0	π	π	−6	13·71	0·304
	or 0	0	0			
3	π	0	π	−10·53	6	0·637
	or π	π	0			
4	π	π	π	−13·71	6	0·696
	or π	0	0			

liquid crystal phases. From considerations of molecular constitution and packing, and of the densities of related aliphatic and aromatic molecules, values for the electron densities (in electrons/Å^3) can be estimated as

$$\varrho_0 = 0{\cdot}33 \pm 0{\cdot}03,$$
$$\varrho_{\text{tail}} = 0{\cdot}26 \pm 0{\cdot}01,$$
$$\varrho_{\text{head}} = 0{\cdot}49 \pm 0{\cdot}04.$$

This gives $r = 0{\cdot}32 \pm 0{\cdot}05$, clearly indicating that either Model 1 or Model 2 is the appropriate model, rather than their inverses (Models 3 and 4), although density criteria are insufficiently exact to differentiate between Models 1 and 2.

Figures 2 and 3 show contour maps and histogram plots of the variation of electron density over various sections through the unit cell for Models 1 and 2. The electron density varies smoothly with position, and there are thus no sharp boundaries between core and tail regions, although the agreement of observed and estimated electron density ratios (r) strongly suggests that the regions of maximum and minimum density are indeed associated with cores and tails, respectively.

Both models have concentrations of electron density at the six face-centre positions and at the body-centre position, with electron density minima at the eight $\frac{1}{4},\frac{1}{4},\frac{1}{4}$ positions. The differences between the two models are best described in terms of the electron densities at points of high symmetry in the unit cell, as shown in table 4. In Model 1, the maxima in $\varrho(\mathbf{r})$ at the face-centre and body-centre positions are almost equal and so, of the two models, Model 1 describes the simpler structure. By choosing the phase of the fourth-strongest reflection, ϕ_{211}, to be π, the peak electron densities at the face-centre and body-centre positions in the unit cell can be made almost identical. Conversely, if ϕ_{211} is chosen to be 0, the difference between the peak electron densities at these positions becomes greater.

Table 4. Comparison of Models 1, 1 (a) and 2.

	Electron density (arbitrary units) at (x,y,z)				
Model	Corner $(0,0,0)$	Edge $(\frac{1}{2},0,0)$	Face centre $(\frac{1}{2},\frac{1}{2},0)$	Body centre $(\frac{1}{2},\frac{1}{2},\frac{1}{2})$	$(\frac{1}{4},\frac{1}{4},\frac{1}{4})$
1	1·46	2·36	9·63	10·53	−6·00
2	−1·71	5·54	6·45	13·71	−6·00
1 (a)	−0·44	2·32	9·87	9·50	−5·77

As indicated in table 2, the remaining two reflections ({200} and {300}) have only a small effect on the final $\varrho(\mathbf{r})$. If the phase factors for the {211}, {220} and {300} reflections are all chosen to be π, then the resulting electron densities at points of high symmetry are as given in table 4 as Model 1 (a). Figure 4 shows contour maps and histogram plots of the variation of electron density $\varrho(\mathbf{r})$ for Model 1 (a). Comparison of Models 1 and 1 (a) (figures 2 and 4) shows that the contribution to $\varrho(\mathbf{r})$ from the {211}, {220} and {300} reflections is relatively minor, and demonstrates that a qualitative description of $\varrho(\mathbf{r})$ can be obtained by considering only the intensities of the three strongest reflections.

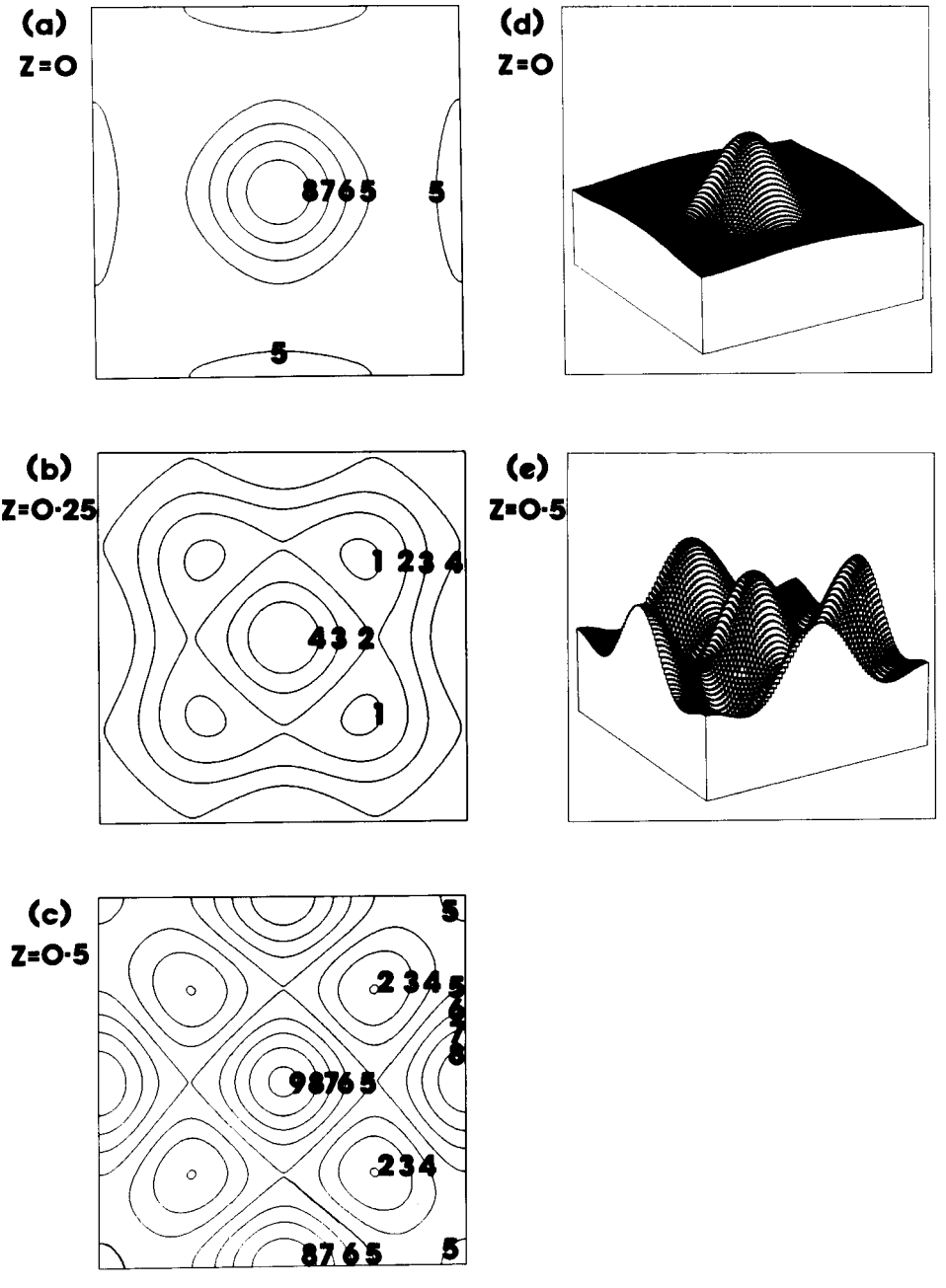

Figure 2. Model 1. Electron density distribution in the unit cell computed from the intensities of the three strongest reflections, with phase factors $\phi_{200} = 0$, $\phi_{111} = 0$ and $\phi_{210} = \pi$. (a, b, c) Contour maps of the electron density distribution $\varrho(x, y) - \varrho_0$ in the xy plane of the unit cell for (a) $z = 0$, (b) $z = \frac{1}{4}$ and (c) $z = \frac{1}{2}$, respectively. Units for $\varrho(x, y)$ are the same as those used in the tables. The contour interval is 2 units. The electron density increases with contour number, and contour number 4 corresponds to $\varrho(x, y) - \varrho_0 = 0$; i.e. $\varrho(x, y) = \varrho_0$. (d, e) Perspective histogram plots showing $\varrho(x, y) - \varrho_0$ for (d) $z = 0$ and (e) $z = \frac{1}{2}$.

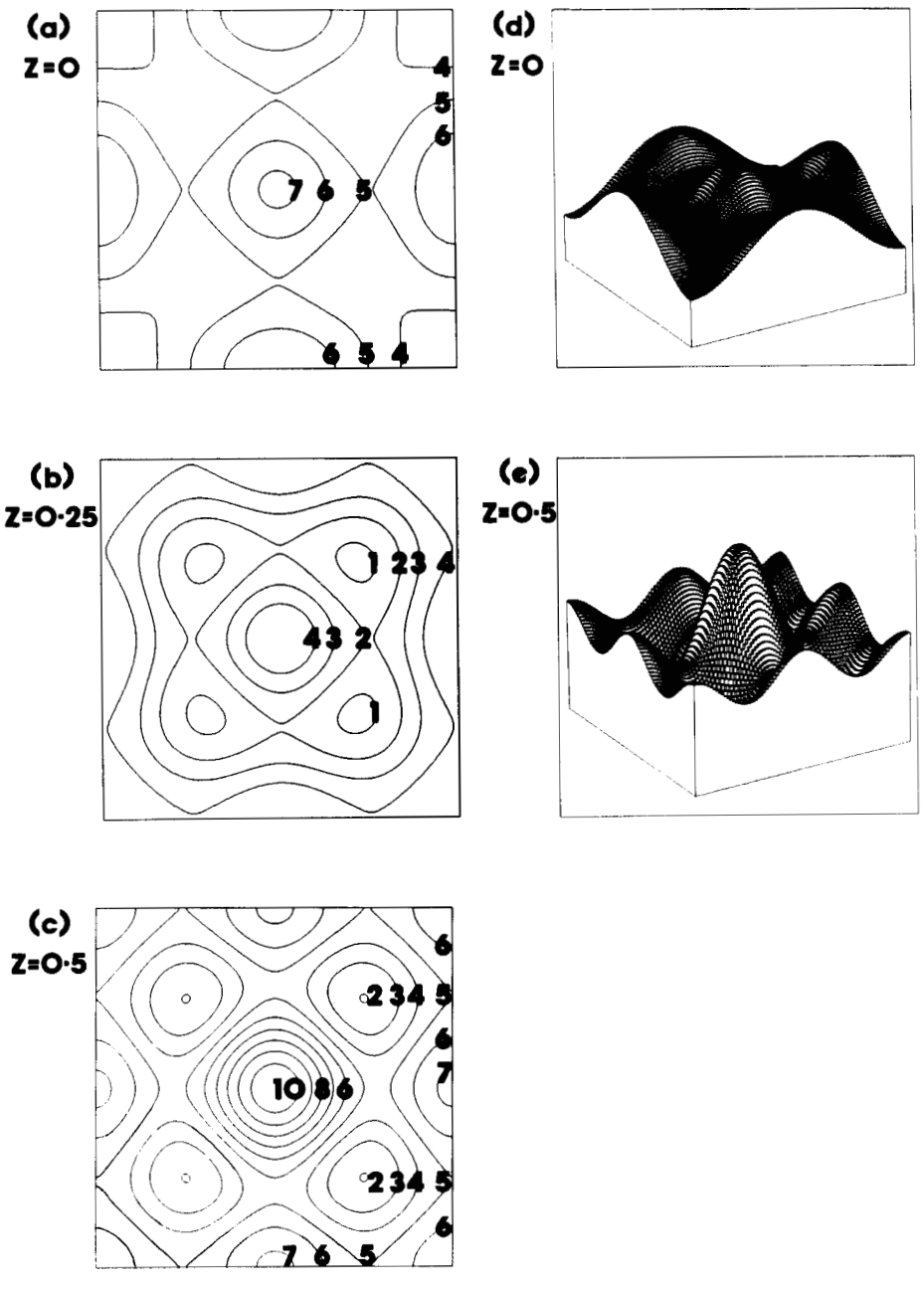

Figure 3. Model 2. Electron density distribution in the unit cell computed from the intensities of the three strongest reflections, with phase factors $\phi_{200} = 0$, $\phi_{111} = \pi$ and $\phi_{210} = \pi$. (a, b, c) Contour maps of the electron density distribution $\varrho(x, y) - \varrho_0$ in the xy plane of the unit cell for (a) $z = 0$, (b) $z = \frac{1}{4}$ and (c) $z = \frac{1}{2}$, respectively. Units for $\varrho(x, y)$ are the same as those used in the tables. The contour interval is 2 units. The electron density increases with contour number, and contour number 4 corresponds to $\varrho(x, y) - \varrho_0 = 0$; i.e. $\varrho(x, y) = \varrho_0$. (d, e) Perspective histogram plots showing $\varrho(x, y) - \varrho_0$ for (d) $z = 0$ and (e) $z = \frac{1}{2}$.

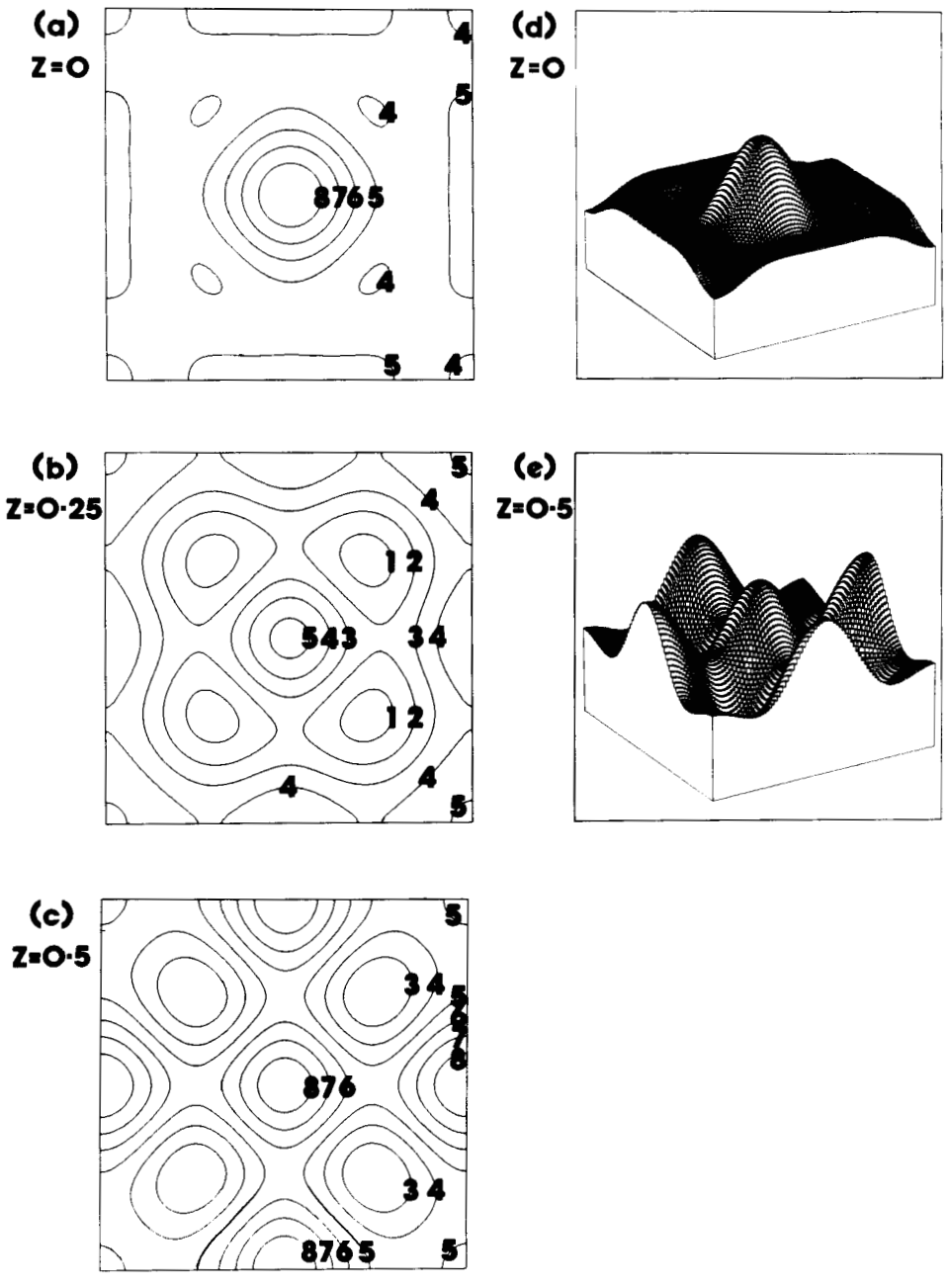

Figure 4. Model 1 (*a*). Electron density distribution in the unit cell computed from all six non-zero reflection intensities, with ϕ_{200}, ϕ_{111} and ϕ_{210} as for Model 1, and the remaining ϕ_{hkl}s equal to π. (*a*, *b*, *c*) Contour maps of the electron density distribution $\varrho(x, y) - \varrho_0$ in the xy plane of the unit cell for (*a*) $z = 0$, (*b*) $z = \frac{1}{4}$ and (*c*) $z = \frac{1}{2}$, respectively. Units for $\varrho(x, y)$ are the same as those used in the tables. The contour interval is 2 units. The electron density increases with contour number, and contour number 4 corresponds to $\varrho(x, y) - \varrho_0 = 0$; i.e. $\varrho(x, y) = \varrho_0$. (*d*, *e*) Perspective histogram plots showing $\varrho(x, y) - \varrho_0$ for (*d*) $z = 0$ and (*e*) $z = \frac{1}{2}$.

3.2.2. *Space group Pm3*

Models 1 and 2 represent structures with the space group Pm3m. As has already been remarked, the apparent differences in I_{210} and I_{120} indicate that the space group could be Pm3 rather than Pm3m (i.e. lacking fourfold symmetry axes). If the phases of the {210} and {120} reflections are taken to be equal, the resulting $\varrho(\mathbf{r})$ is almost identical to those for Models 1 and 2, and so this case need be discussed no further. If the phases of the {210} and {120} reflections are different, however, a very different $\varrho(\mathbf{r})$ results. The exact choice of these phases has little effect on $\varrho(\mathbf{r})$ since the $\varrho(\mathbf{r})$ functions resulting from the two alternative choices of phases (i.e. $\phi_{210} = 0$ and $\phi_{120} = \pi$, or $\phi_{210} = \pi$ and $\phi_{120} = 0$) are almost identical after rotation by 90° about one of the twofold axes. These findings are summarized in table 5, which shows the contribution to $\varrho(\mathbf{r})$ from the {210} and {120} reflections with the various combinations of phases discussed previously.

Table 5. Contribution to $\varrho(\mathbf{r})$ at points of high symmetry in the unit cell from the {210} (and {120}) reflections for space groups Pm3m and Pm3, as a function of the phase factors ϕ_{210} and ϕ_{120}.

			Electron density (arbitrary units) at (x, y, z)				
Space Group	ϕ_{210}	ϕ_{120}	Corner (0,0,0)	Edge $(\frac{1}{2},0,0)$	Face centre $(\frac{1}{2},\frac{1}{2},0)$	Body centre $(\frac{1}{2},\frac{1}{2},\frac{1}{2})$	$(\frac{1}{4},\frac{1}{4},\frac{1}{4})$
Pm3m†	0	–	6·13	2·03	−2·03	−6·13	−0·38
Pm3‡	0	0	6·08	2·02	−2·02	−6·08	−0·37
Pm3‡§	0	π	0·61	0·20	−0·20	−0·61	−0·03
Pm3‡‖	π	0	−0·61	−0·20	0·20	0·61	0·03

† $I_{210} = 0{\cdot}065$.

‡ $I_{210} = 0{\cdot}078$, $I_{120} = 0{\cdot}052$.

§ $\varrho_{\min} = -4{\cdot}06$ at the 12 cyclically permuted positions $\frac{1}{4},\frac{1}{2},0$; $\varrho_{\max} = +4{\cdot}06$ at the 12 cyclically permuted positions $\frac{1}{4},0,\frac{1}{2}$.

‖ $\varrho_{\min} = -4{\cdot}06$ at the 12 cyclically permuted positions $\frac{1}{4},0,\frac{1}{2}$; $\varrho_{\max} = +4{\cdot}06$ at the 12 cyclically permuted positions $\frac{1}{4},\frac{1}{2},0$.

Thus if the space group is Pm3 and it is assumed that the phases of the {210} and the {120} reflections are not equal, then two more models for $\varrho(\mathbf{r})$ (Models 5 and 6) result. (The additional models, which are the inverses of Models 5 and 6, can be rejected for the same reasons that Models 3 and 4 were rejected.) The electron density functions $\varrho(\mathbf{r})$ for Models 5 and 6 are shown in figures 5 and 6. These are clearly more complex than for Models 1 and 2, but show qualitative similarities between themselves, with regions of high electron density at the corners, edges, and face-centre and body-centre positions, and minima at the $\frac{1}{4},\frac{1}{4},\frac{1}{4}$ positions. Both models have approximately spherical concentrations of electron density at the body-centre and corner positions in the unit cell. In Model 5 the peak electron density is higher at the corners than at the body-centre position, whereas for Model 6 the peak electron density is higher at the body-centre position. Both models possess regions of electron density which may be described in terms of a network of infinite non-uniform rods. The rods lie in the faces of the unit cell with their axes along the [100], [010] and [001] directions, and are non-intersecting. For Model 5 the peak in electron density within these rods occurs at the face-centre position, while for Model 6 it occurs at the edge position.

The values of the electron density ratio r for Models 5 and 6 are 0·435 and 0·422, which are significantly higher than the value $0{\cdot}32 \pm 0{\cdot}05$ calculated for the case where

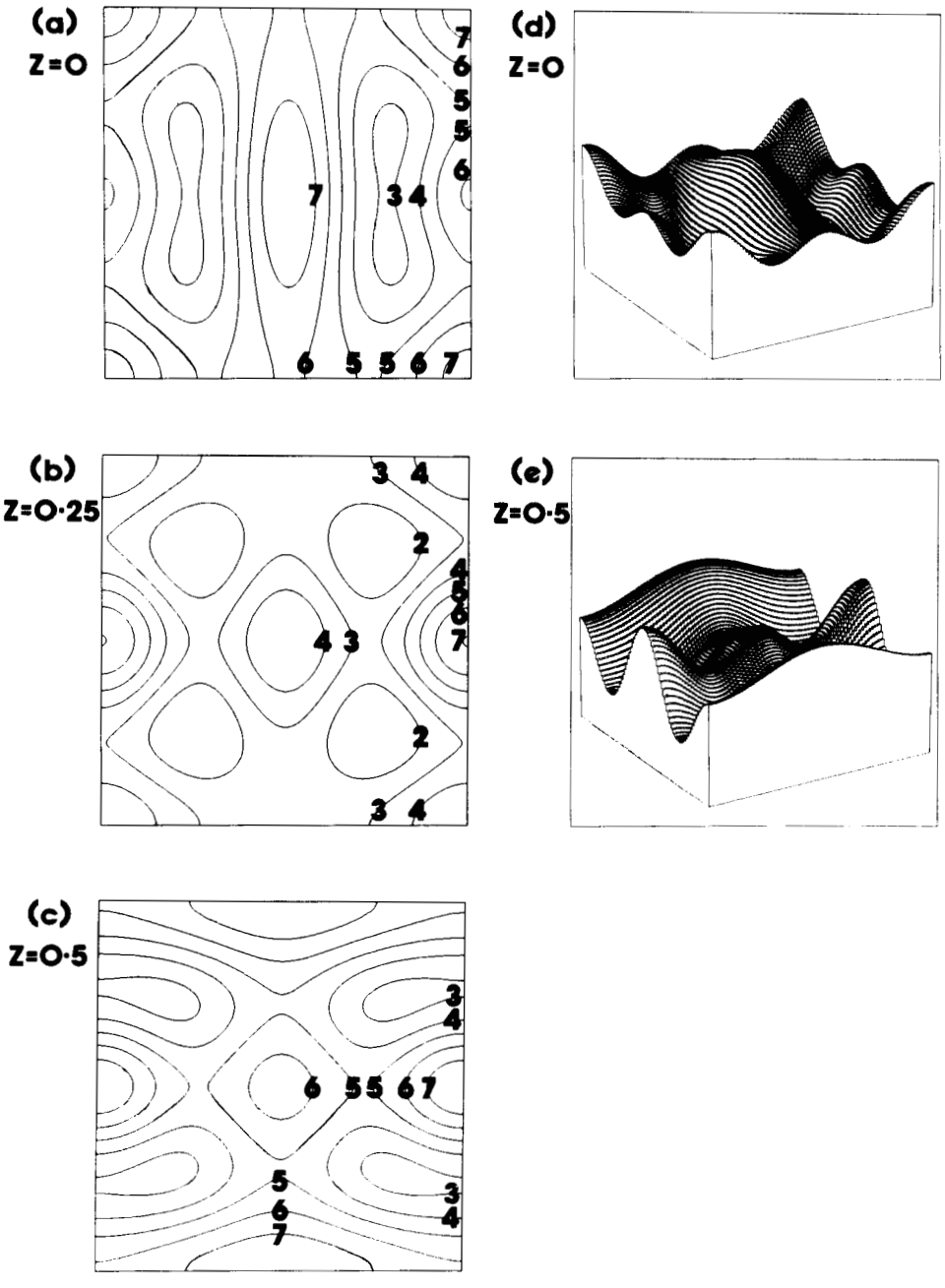

Figure 5. Model 5. Electron density distribution in the unit cell computed from the intensities of the three strongest reflections, with phase factors $\phi_{200} = 0$, $\phi_{111} = 0$, $\phi_{210} = \pi$ and $\phi_{120} = 0$. (a, b, c) Contour maps of the electron density distribution $\varrho(x, y) - \varrho_0$ in the xy plane of the unit cell for (a) $z = 0$, (b) $z = \frac{1}{4}$ and (c) $z = \frac{1}{2}$, respectively. Units for $\varrho(x, y)$ are the same as those used in the tables. The contour interval is 2 units. The electron density increases with contour number, and contour number 4 corresponds to $\varrho(x, y) - \varrho_0 = 0$; i.e. $\varrho(x, y) = \varrho_0$. (d, e) Perspective histogram plots showing $\varrho(x, y) - \varrho_0$ for (d) $z = 0$ and (e) $z = \frac{1}{2}$.

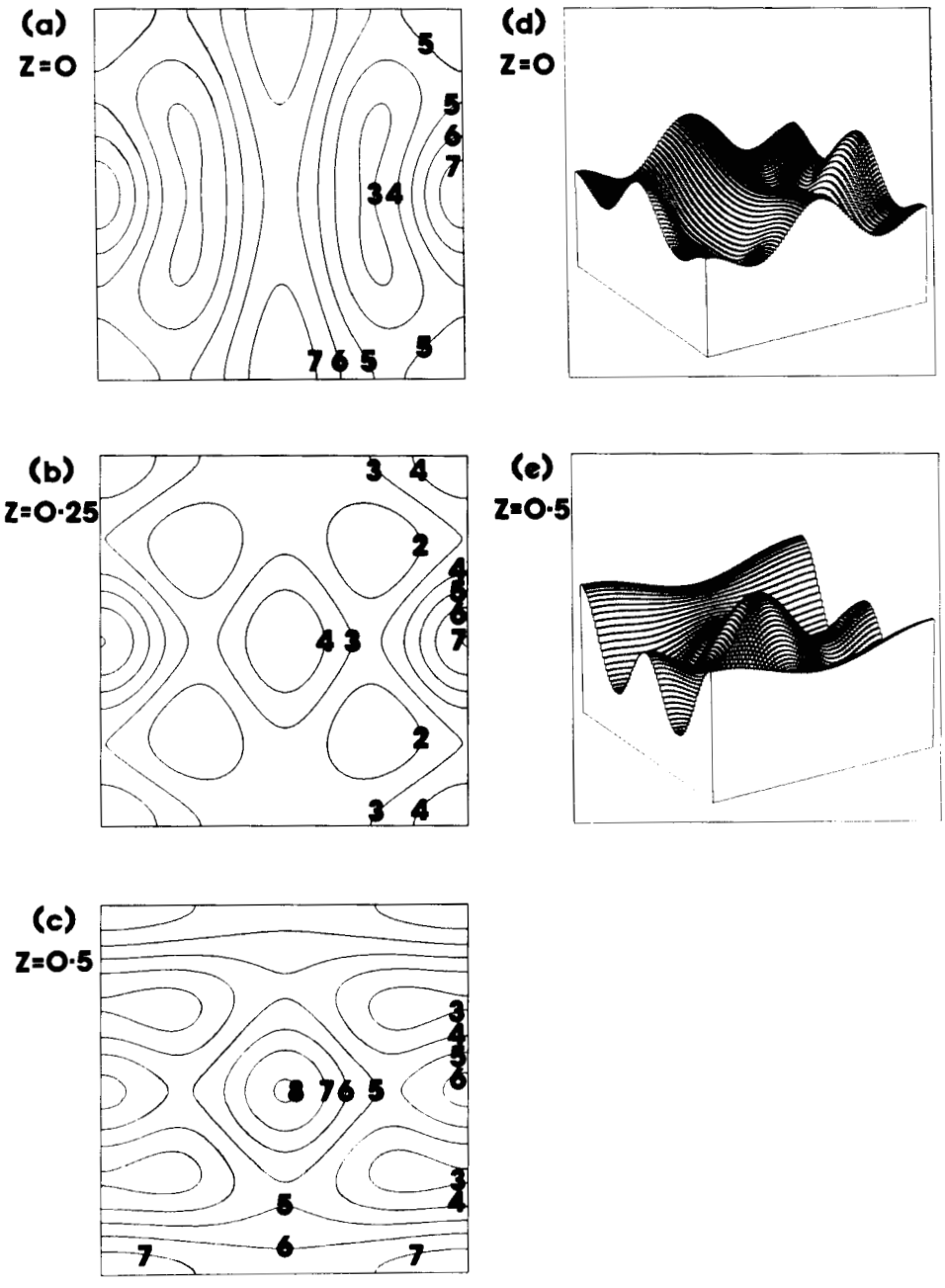

Figure 6. Model 6. Electron density distribution in the unit cell computed from the intensities of the three strongest reflections, with phase factors $\phi_{200} = 0$, $\phi_{111} = \pi$, $\phi_{210} = \pi$ and $\phi_{120} = 0$. (*a*, *b*, *c*) Contour maps of the electron density distribution $\varrho(x, y) - \varrho_0$ in the *xy* plane of the unit cell for (*a*) $z = 0$, (*b*) $z = \frac{1}{4}$ and (*c*) $z = \frac{1}{2}$, respectively. Units for $\varrho(x, y)$ are the same as those used in the tables. The contour interval is 2 units. The electron density increases with contour number, and contour number 4 corresponds to $\varrho(x, y) - \varrho_0 = 0$; i.e. $\varrho(x, y) = \varrho_0$. (*d*, *e*) Perspective histogram plots showing $\varrho(x, y) - \varrho_0$ for (*d*) $z = 0$ and (*e*) $z = \frac{1}{2}$.

the extremes of electron density correspond to molecular cores and tails. Higher values can result if there is some admixture of tails throughout the mainly core regions, which clearly cannot be ruled out. Models 5 and 6 cannot therefore be excluded on the basis of their electron density ratio, although it does make them less probable than Models 1 and 2.

To summarize, if the space group is Pm3m, or Pm3 with $\phi_{210} = \phi_{120}$, then the correct model for $\varrho(\mathbf{r})$ is either Model 1 or Model 2. If the space group is Pm3 and $\phi_{210} \neq \phi_{120}$, then the correct model is either Model 5 or Model 6. Parameters for the four models are summarized in Table 6.

Table 6. Summary of parameters for Models 1, 2, 5 and 6. $I_{200} = 1{\cdot}0000$ and $I_{111} = 0{\cdot}0395$.

Model	Space group	ϕ_{200}	ϕ_{111}	ϕ_{210}	ϕ_{120}	I_{210}	I_{120}
1	Pm3m	0	0	π	–	0·065	0·065
2	Pm3m	0	π	π	–	0·065	0·065
5	Pm3	0	0	π	0	0·078	0·052
6	Pm3	0	π	π	0	0·078	0·052

3.2.3. *Physical interpretation*

The broad diffraction maximum measured at a d spacing of approximately 4·8 Å shows that there are only liquid-like correlations between molecules. The crystalline diffraction pattern results from cubic long-range ordering (over a distance of at least 800 Å) of relatively large regions of high and low electron density, with a unit cell parameter of 86 Å. These regions may be thought of as a soft (i.e. slowly varying) three-dimensional density wave, having only a small number of Fourier components. While the D phase cannot be classified as smectic, there is clearly a similarity with the smectic A and C phases, the structures of which may be described in terms of a one-dimensional density wave with only one or two Fourier components of significant magnitude.

As discussed previously, the variation in electron density over the unit cell must result from a variation in the ratio of the concentration of aromatic core groups to aliphatic tail groups as a function of position in the unit cell. It may be supposed that regions of maximum electron density contain only core groups, while regions with minimum electron density contain only tail groups, with a continuous variation in the concentration ratio in between. The structure is thus truly a liquid crystal, with a liquid-like molecular packing modulated by the association of cores and tails with a three-dimensional periodicity.

The presence of carboxylic acid groups must result in the molecules being associated as dimers (or polymers) by hydrogen bonding. Direct confirmation of this is found from the measured d spacing of 48 Å in the S_C phase of this material. This may be compared with the maximum single molecular length L of 34·9 Å, as measured from a molecular model, or twice this figure for a dimer. The latter value gives a molecular tilt angle of 47°, from $\cos^{-1}(d/L)$.

More importantly, however, as may be seen from the figures, the distance between the maximum and minimum values of electron density for all the models is consistent with the dimensions of molecular dimers. In Model 1, for example, maxima occur at body-centre and face-centre positions and minima at the $\frac{1}{4},\frac{1}{4},\frac{1}{4}$, positions. The distance between these maxima and minima is about 37 Å, as compared with the molecular length of 35 Å.

The variation of electron density clearly results from the mutual association of aromatic and of aliphatic groups. However, the rare occurrence of the D phase and the fact that it occurs only in compounds having a strong outboard dipole (–CN or $-NO_2$) strongly suggests that the presence of these groups is a prerequisite for D phase formation. It may be that the ability of these groups to form hydrogen bonds promotes the formation of the large aromatic groupings found in the D phase.

4. Conclusions

The electron density function $\varrho(\mathbf{r})$ for four distinct and physically reasonable models of the D phase of 4-*n*-octadecyloxy-3′-cyanobiphenyl-4-carboxylic acid has been calculated by a Fourier analysis of X-ray diffraction intensity measurements. All the models have primitive cubic symmetry. On the basis of the available data, each of the four models must be regarded as a possible representation of the structure. Models 1 and 2 may be described as linked spherical micelles clustering around the body-centre and face-centre positions in the unit cell. Of these, Model 1 is conceptually simpler since it has approximately equal concentrations of head groups in these two positions. In addition, it is consistent with a structure in which the peaks in the electron density function $\varrho(\mathbf{r})$ correspond to the presence of head groups only, while the minima in $\varrho(\mathbf{r})$ correspond to the presence of tail groups only. Models 5 and 6 have approximately spherical concentrations of electron density at the edges and body-centre positions in the unit cell, and also possess features that may be described as sets of orthogonal, infinite, non-uniform unconnected rods. These models have lower symmetry than Models 1 and 2, and the molecular cores and tails appear to be less separated than in the more symmetric models.

The authors would like to thank Mr. W. T. Toner of the Laser Division, Rutherford Appleton Laboratory, for providing facilities for measuring optical second harmonic generation.

References

[1] ETHERINGTON, G., LEADBETTER, A. J., WANG, X. J., GRAY, G. W., and TAJBAKHSH, A., 1986, *Liq. Crystals*, **1**, 209.
[2] NYE, J. F., 1957, *Physical Properties of Crystals* (Oxford University Press), Chap. 7.
[3] TARDIEU, A., and BILLARD, J., 1976, *J. Phys., Paris*, **37**, C3–79.
[4] DIELE, S., BRAND, P., and SACKMANN, H., 1972, *Molec. Crystals liq. Crystals*, **17**, 163.
[5] MACKAY, A. L., 1985, *Nature, Lond.*, **314**, 604.
[6] HYDE, S. T., and ANDERSSON, S., 1984, *Z. Kristallogr.*, **168**, 221.